CrossMark

RESEARCH PAPER

Characterization and evaluation of 3D printed microfluidic chip for cell processing

Jia Min Lee[1] · Meng Zhang[1] · Wai Yee Yeong[1]

Abstract Microfluidics has found ubiquitous presence in biological applications such as tissue spheroid fabrication and pharmacology investigation. The increasing prevalence and complexity demand a highly adaptable fabrication method for the rapid and convenient production of these microfluidic systems. 3D printing, as an emerging fabrication technique, was investigated in this paper. Microfluidic features were fabricated using two most widely used 3D printing technologies namely the inkjet printing and filament deposition techniques. The printing resolution, accuracy, repeatability, surface roughness, wetting ability, and biocompatibility of the printed microfluidic chips were characterized. The capability of 3D printing was demonstrated by printing a number of microfluidic devices such as rotational flow device and gradient generator. Results showed that 3D printing techniques were successful in making intricate microscale architectures and have the potential of greatly simplifying the manufacturing process.

Keywords 3D printing · Additive manufacturing · Rapid prototyping · Microfluidics · Material characterization · Cells · Tissue engineering

1 Introduction

First developed in the 1970s as a gas chromatograph, the microfluidics, also known as lab-on-chips or micrototal analysis systems (μTAS), has been explored by various industries for diverse applications. In particular, some biological applications include cell sorting and isolation (Benavente-Babace et al. 2014; Holmes et al. 2014; Nagrath et al. 2007), biosensor and diagnostic (Moltzahn et al. 2011; Shih et al. 2013; Yan et al. 2011), pharmacological testing (Kuo et al. 2014; Novik et al. 2010), and bioreactor for coculture and maturation of microorgans. Moreover, several performances can be integrated within a single chip which isolate cells and perform DNA analysis (qPCR) (Rival et al. 2014). The application of microfluidic systems in tissue engineering studies includes processing of biomaterials [microbeads (Wang et al. 2011) or microfibers (Kang et al. 2011; Onoe et al. 2013)] and cell sorting and focusing (Bhagat et al. 2008; Huang et al. 2004; Yamada et al. 2004)].

In addition, multi-cellular tissue spheroid formation is an area that has garnered much attention for a variety of applications, including drug testing in cancer research and more recently as the building block for the 3D printing of organs. Hence, microfluidic design such as physical traps (Wu et al. 2008), rotation flow of two parallel inlet channels with opposite flows (Ota et al. 2010a, b, 2011; Takai et al. 2013a, b) and droplet-based encapsulating microfluidic device have been widely investigated (Chan et al. 2013; Sakai et al. 2011; Yu et al. 2010).

For biological applications, the dimensions in microfluidics are generally designed in the range of 100–1000 microns, unless single-cell analysis is intended for the microfluidic chip which requires small scales (Young and Beebe 2010). The fabrication of most microfluidic chips relies on photolithography technology with elastomeric material, such as poly (dimethylsiloxane) (PDMS), for making the microfluidic device. Other fabrication methods include embossing, injection molding, and laser ablation (Fiorini and Chiu

✉ Wai Yee Yeong
wyyeong@ntu.edu.sg

1 Centre for 3D Printing, School of Mechanical and Aerospace Engineering, Nanyang Technological University, 50 Nanyang Avenue, Singapore 639798, Singapore

2005). Such fabrication methods generally produce microfluidic chips with two-dimensional (2D) planar designs (Capel et al. 2013). More intricate designs would lead to increased manufacturing complexity through methods such as direct projection on dry-film photoresist (Zhao et al. 2009), 'membrane sandwich' method (Anderson et al. 2000a), and the femtosecond laser direct writing (Liao et al. 2012).

Additive manufacturing (AM) technique, also known as 3D printing, may serve as an alternative fabrication tool due to its ability to produce complex and multi-level geometry (Chua et al. 2005; Khoo et al 2015; Vaezi and Yang 2015; Yeong et al. 2005). Various materials can be used in 3D printing including hydrogels, polymers, metals, and ceramics (Lee and Yeong 2015; Sing et al. 2015; Wang et al. 2015; Yeong et al. 2004, 2014). The printing of microchips was pioneered by McDonald et al. (2002) who investigated the printing of templates for PDMS casting using a solid-based printer. One of the first direct printing of microchip was accomplished by Moore et al, involving microfluidic compact disk (Moore et al. 2011). The versatility of 3D printing has also spurred the development of auxiliary components, e.g., the 3D-printed microchip interconnect with gasket and clipping mechanism, which was designed for addressing issues at the world-to-chip interface (Paydar et al. 2014). 3D-printed microfluidic chips can integrate intricate features such as membrane-like valve within the microchannels to regulate fluid flow (Au et al. 2015; Rogers et al. 2015).

A number of works, as summarized in Table 1, characterizes 3D-printed microfluidic systems, in terms of the geometrical aspects and surface conditions of the printed parts, using a variety of printers and build materials. These works did not provide a comprehensive examination of microfluidic features, e.g., slanted channels, and the printing repeatability, which is a key factor for evaluating the performance of a printer. The current work describes the design, fabrication, and characterization of microfluidic chip features for evaluating the applicability of 3D printing for making tissue engineering-based microfluidic platforms. Printing resolution, accuracy, and repeatability were examined. Surface roughness and water wetting ability were evaluated. Biocompatibility of the printed pieces under a number of treatment conditions was investigated. The paper also discusses some limitations and design criteria of 3D-printed microfluidic chips.

2 Materials and methods

2.1 The printing process

The inkjet printer used is the Object Eden350V (Stratasys) with FullCure 720 model material and FullCure 705 support material. Briefly, the STL files of the parts were imported to the printer software Object Studio. The glossy mode was selected for printing of the parts. The completed parts were washed with water jet and subsequently immersed in ultrasonic bath (Sonorex Super) for 10 min for the removal of the support material (Yap and Yeong 2015).

The fused deposition modeling printer (FDM) used is Dimension Elite (Stratasys) with ABSplus-P430 filament as the model material and P400SR filament as the support material. A layer thickness of 0.178 mm was selected for printing. The CatalystEx software converted the STL file into the print paths. The support materials were removed using the SCA-1200 support removal system, which involves the soaking of the printed parts in aqueous sodium hydroxide (70 % w/v NaOH) overnight.

2.2 Design of microfluidic chips

The test piece was designed using SolidWorks 2014 CAD software and exported in the STL format (Fig. 1). Features were measured for the evaluation of printing resolution, accuracy, circularity, surface roughness, and water contact angle.

2.3 Characterization

All physical measurements were performed at least five times to achieve statistically significant results. For qualitative results, the scanning electron microscope (Jeol JSM 5600-LV) and inverted microscope (Olympus Inverted Microscope CKX41) were used. Image J Software was used to quantify and measure the dimensions of printed part.

2.3.1 Printer repeatability testing

The printer repeatability in terms of the printing accuracy between parts in a single build on different locations of the printer platform was done for Trench X, Y and Z with nominal dimensions of 400 µm in all three axes. Each of the features was printed five times at random locations on the printer platform. Single-factor ANOVA was performed.

2.3.2 Surface roughness measurement

Surface roughness was measured using the Plµ Sensofar confocal image profiler. The available system is capable of profiling a maximum slope of 51° using a 100 × EPI objective for a smooth surface, and a maximum field of view was 700 × 525 µm² with a 20 × EPI objective for a single-profile measurement. This system provides non-contact, nondestructive fast sampling of high aspect ratio and steep samples.

2.3.3 Water contact angle measurement

The contact angle measurements were made using the Attension Theta optical tensiometer and the accompanied software from Biolin Scientific. Five microliters of distilled water was dispensed onto the printed platform for examination.

Table 1 Current works on characterizing 3D printers for microfluidic application

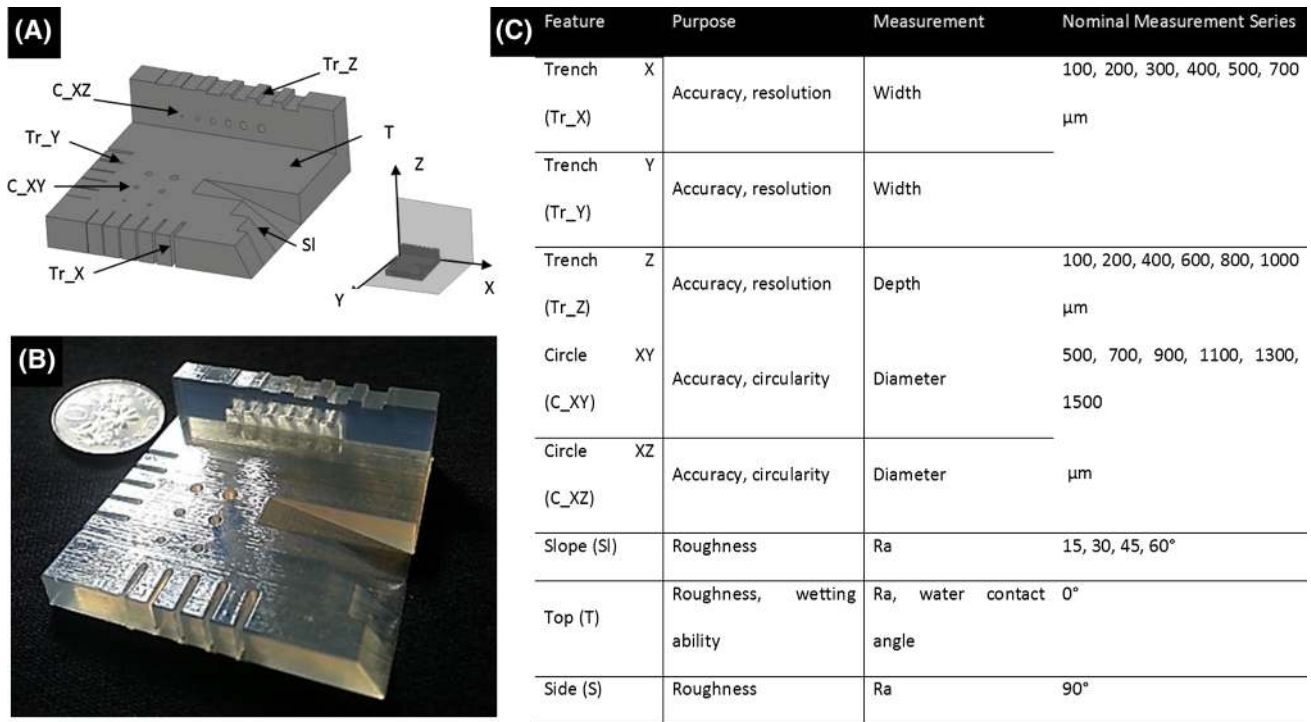| Printing technology	System	Materials + purpose	Resolution	Surface roughness	Accuracy	Advantages and disadvantages (if possible)	References
Binder jetting	VX500 (Voxeljet Technology GmbH, Augsburg, Germany)	Solupor (Voxeljet, Augsburg, Germany)	300 μm for walls and bars, 500 μm for cylindrical beams and 100 μm for holes	60 μm for non-infiltrated samples	Different depending on the geometric features, but may reach up to 300 μm	Material shrinkage during polymerization; Lower material strength than that produced by conventional methods; Infiltration needed to improve material strength and surface properties	Polzin et al. (2013)
Inkjet printing	HD3500+ (University of Auckland, New Zealand)	VisiJet Crystal (3D Systems, Australia)	–	Stitch marks are present	506 ± 8 μm (nominal dimension 500 μm)	Optically transparent, facilitates on-chip visualization of cells; Tested treatment methods does not provide high bio-compatibility	Zhu et al. (2013)
Stereolithography (SLA)	Viper Pro (Plastic Design Technology, Auckland, New Zealand)	Watershed 11122 XC (Watershed) and Dreve Fototec 7150 Clear (Dreve Otoplastik GmbH)	–	Scanline pattern is present	370 ± 39 μm (nominal dimension 500 μm)	Optically transparent, facilitates on-chip visualization of cells; Tested treatment methods does not provide high bio-compatibility	Zhu et al. (2013)
Digital Light Processing (DLP)	Miicraft (Miicraft, Hsinchu, Taiwan)	A proprietary colorless resin	250 μm	Less than 1 to 10 μm, depending on the side	50–100 μm narrower than nominal dimensions	Accuracy affected by exposure time and intensity	Shallan et al. (2014)

(C) Feature		Purpose	Measurement	Nominal Measurement Series
Trench (Tr_X)	X	Accuracy, resolution	Width	100, 200, 300, 400, 500, 700 µm
Trench (Tr_Y)	Y	Accuracy, resolution	Width	
Trench (Tr_Z)	Z	Accuracy, resolution	Depth	100, 200, 400, 600, 800, 1000 µm
Circle (C_XY)	XY	Accuracy, circularity	Diameter	500, 700, 900, 1100, 1300, 1500
Circle (C_XZ)	XZ	Accuracy, circularity	Diameter	µm
Slope (Sl)		Roughness	Ra	15, 30, 45, 60°
Top (T)		Roughness, wetting ability	Ra, water contact angle	0°
Side (S)		Roughness	Ra	90°

Fig. 1 **a** CAD drawing of the testing parts and the orientation of print. **b** Sample of printed parts using inkjet printer. **c** Features measurement

2.3.4 Biocompatibility test of model materials

In total, 0.7×10^6 cells C2C12 cells were seeded onto printed samples (circular disk: 400 mm² × 2 mm) that have undergone process conditions stated in Table 2. The samples were incubated at 37 °C overnight in a 5 % CO_2 incubator in medium (Dulbecco's modified Eagle medium (Serana), 10 % Fetal Bovine Serum, 1 % Antibiotics). Subsequently, cells were prepared for fluorescence staining using the Live/Dead Cell Double Staining Kit (Sigma-Aldrich®). Cell viability was assessed using fluorescence microscopy and quantified using ImageJ software. Sterilization conditions using UV and 70 % ethanol were investigated. Other sterilization method such as high-temperature autoclaving (120 °C, 20 min) was not chosen due to the polymer low melting temperature (~60 °C for FullCure 720).

3 Results and discussion

3.1 Simplified process of 3D-printed microfluidic devices

This paper provides a systematic layout of steps in 3D printing of microfluidic chips. Through this case study, we showed that process chain of microfluidic fabrication can

Table 2 Sterilization condition

Sterilization condition	Duration
UV exposure	1 h
70 % Ethanol	0.5 h
UV exposure + 70 % ethanol	1 h followed by 0.5 h respectively

now be simplified into three major steps, namely pre-printing, printing, and post-printing stages (Fig. 2). This study also provides a comprehensive outline of design and process selection criteria in 3D-printed microfluidic chips for general biological and cell-based applications.

3.2 Printing resolution, accuracy, and circularity

For tissue engineering applications, resolution and accuracy of the fabricated chips are essential considering the fact that cells are in the order of 20 µm. For example, passive particle separation devices such as the deterministic lateral displacement device rely on cell size as the basis for fractionation (Huang et al. 2004). Channel aspect ratio (AR) was found to play a role in directing flows in a stacked 3D device (Ismagilov et al. 2001), as changes in AR impact the relative resistance encountered at the intersection between crossing conduit.
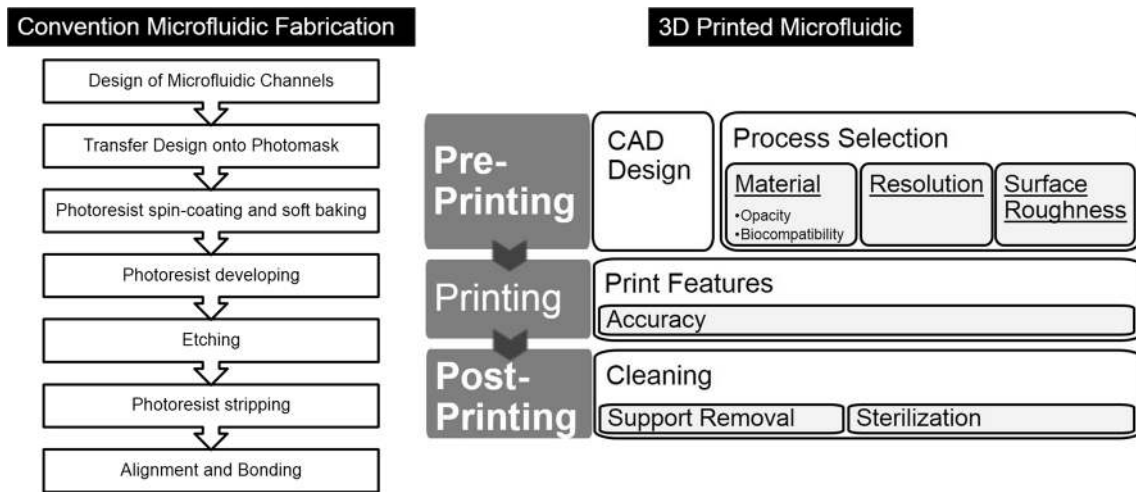
Fig. 2 Comparison of microfluidic chip fabrication using conventional lithography method 3D printing. Design criteria and process selection are also shown in the flow chart for 3D

Preliminary tests were performed for determining the resolution of printing in all three axes (Fig. 3). No observable feature is shown in channel with nominal x and z dimensions of 100 and 500 μm, respectively. In comparison, when channel with nominal x and z dimensions of 500 and 100 μm are printed, observable features were formed, indicating a better resolution in the z-axis for the polyjet. For the FDM printer, the quality of printing at 100 μm is unsatisfactory. As shown in Fig. 4a, which gives the top view of three printed open channels (black regions), dimensions are not consistent along the length.

The results for accuracy of printing are shown in Fig. 5. The accuracy of measured diameters was examined by comparing with the nominal diameters in both the horizontal and vertical planes. The polyjet printer produced better spatial accuracy in all three axes. Specifically, it has an average deviation[1] of 25.2 μm across all measurement series, as compared to 67.8 μm for FDM. In particular, for the polyjet printer, the z-axis was found to have the best accuracy of 8.3-μm deviation, while the x-axis was the least accurate with a deviation of 36.5 μm.

For the FDM printer, the average deviation across all dimensions in the y-axis is 60.8 μm (v–v), which is more accurate than the x-axis's result of 71.5 μm, while for the polyjet printer, y-axis printing was also found to be more accurate, with a result of 30.7 μm. The same observation was made by Shallan et al. (2014) who had experimented using the Objet Geometries Eden 250 polyjet printer and the same printing materials, and they suggested that this could be due to the incorrect labeling of the printing axes in the supplied software of the printer. Such possibility cannot be ruled out, though it could also be a result of measurement error due to small sample size.

Also, parts made by the inkjet printer tend to have leaning sides and rounded corners, as shown in Figs. 3 and 6, which exemplifies this observation using a 500×500 μm^2 ($x \times z$) open channel. Firstly, it could be due to the more viscous nature of the photopolymer and longer solidification time as compared to the FDM material, which causes the printing material to flow to the bottom of the channel under gravity before photopolymerization occured. Secondly, since an open channel with a relatively small dimension was printed, no support material was deposited to confine the build printing material, thus accuracy of the resulting printed feature was negatively impacted. These also explain the consistently smaller dimensions obtained than the theoretical values in the inkjet printer. This is the inherent process limitation of inkjet droplet-based technique in creating delicate fine features.

In general, the 3D-printed microfluidic features showed deviation from the nominal value, which was observed in both inkjet-based and filament-based techniques. Fine features such as small channels of 10–20 μm can be printed successfully, and these length scales are comparable in size to human cells. Features larger than 100 μm can be fabricated with varying degree of accuracies, depending on the orientation of the parts on the build platform and the type of printer used. For the polyjet printer, the use of the z-axis as the dominant printing direction is advised for maximum feature size accuracy, followed by the y-axis. The FDM printer yields less accurate printing as compared to polyjet printing. The results obtained in this section provide reference for the amount of compensation that needs to be made during the design phase of 3D printed microfluidic devices.

---

[1] The deviation or the estimation bias of a measurement series is defined as $\frac{1}{N} \sum_{i=1}^{N} \widehat{\phi}_i - \phi$, where ϕ is the theoretical value, $\widehat{\phi}$ is the measured value.
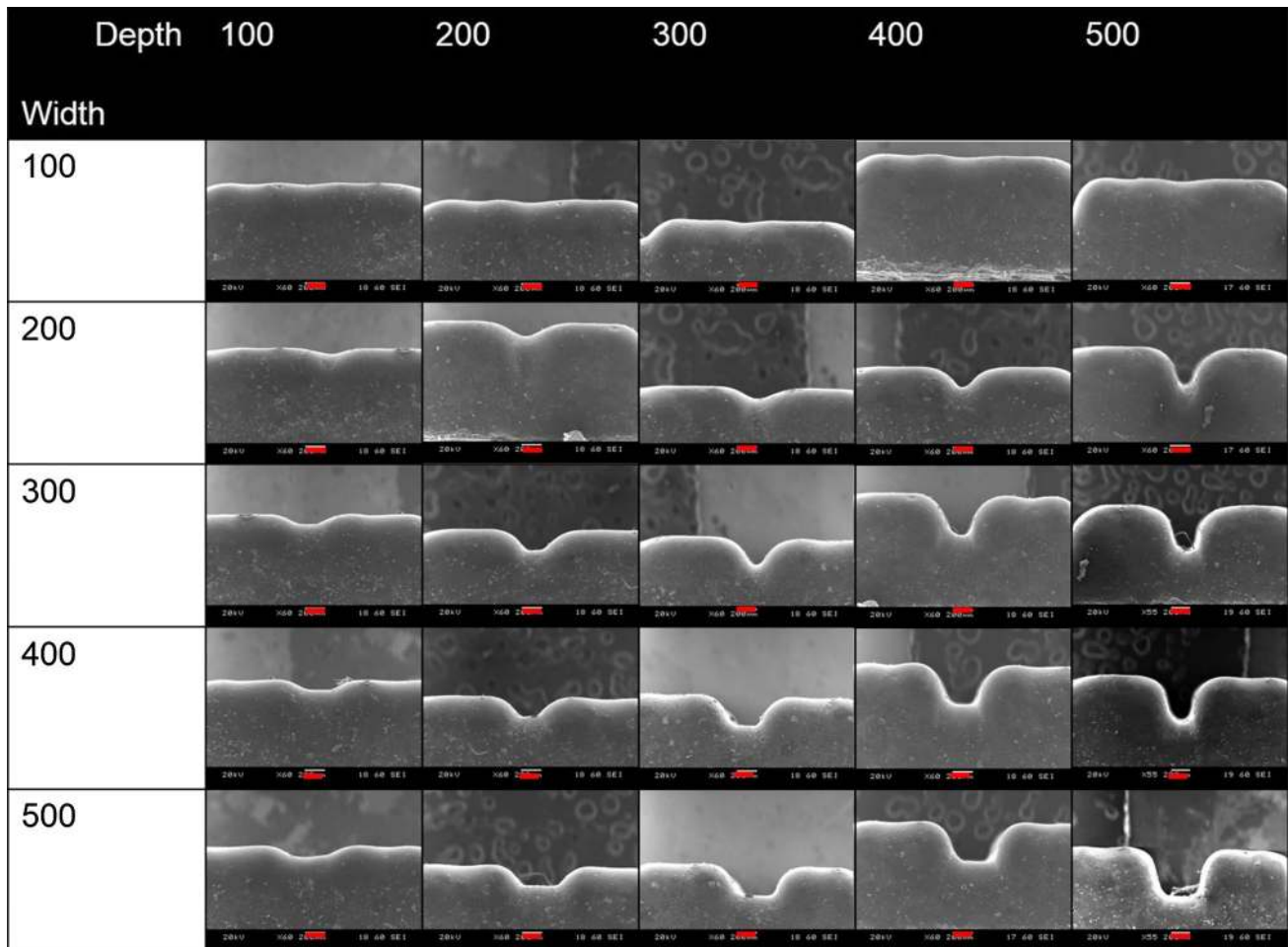
Fig. 3 SEM images of polyjet-printed features (*Red Scale Bar* 200 μm) (color figure online)

3.3 Printing repeatability

At 95 % confidence level, it was shown that the location of parts on the platform has insignificant effect on their accuracy for all three axes. This result validates that the design of the test part does not contribute to the difference in accuracy readings obtained at the dimensions measured (all features are printed on a single piece, so are printed at different locations on the build platform).

3.4 Surface roughness of printed features

As systems decrease in size, near-wall forces become the crucial factors in influencing flow. Surface roughness-induced phenomena, for example, the van der Waals, electrostatic, and steric forces emerge and were believed to offer explanations for observations that are unique to microscale flows (Ho and Tai 1998). Surface roughness influences the friction in microchannel flow (Sun et al. 2012). In biological studies that involve cell manipulation,

lower flow-induced shear stress is ideal (Shen et al. 2014). For example, shear stress was found to have negative impact by causing transient pores to form on cell membrane (Cui et al. 2010). However, parameters associated with such cases are difficult to quantify, as a number of factors such as exposure time to stress, fluid viscosity, and physiology of the cells act to complicate the process (Malda et al. 2013). Comparing with the standard practice, untreated PDMS made using photolithographic casting was found to have an average roughness of 0.68 nm (Schrott et al. 2009). CO_2 laser cutting of polymethyl methacrylate (PMMA) microfluidic surfaces was able to yield a best roughness value of 100.86 nm with appropriate treatment (Huang et al. 2010).

As shown in Fig. 7, the polyjet printer produces relatively smooth features. The surface roughness increases with increasing side wall angle due to the stitch marks formed, as shown in Fig. 7b. From the plot of surface roughness test in Fig. 8, there were more irregular profile at 60° as compared to that at 15°. In fact, such trend
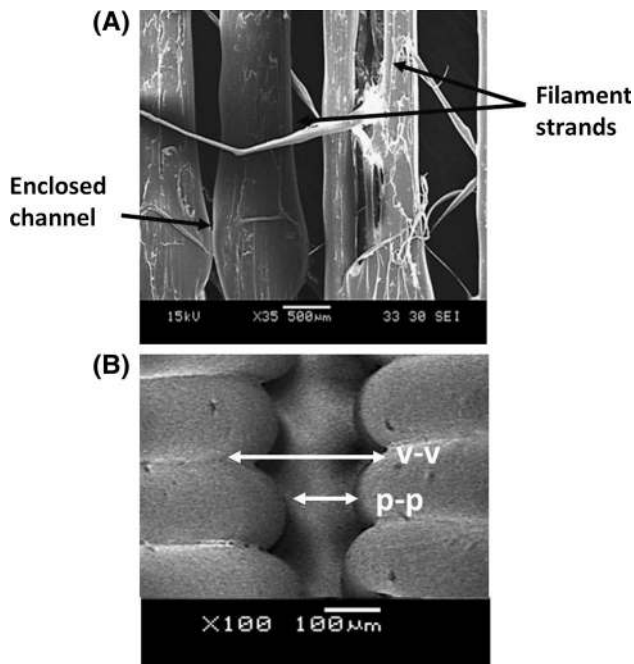
Fig. 4 Channels printed by FDM printer. **a** CAD drawing of the benchmark sample. **b** Top view of the channel. **c** Side view showing a layer by layer structure v (valley) describe

is consistent for the spectrum for angles from 0° to 60°, which ranges from 0.47 to 8.44 μm. However, roughness at 90° decreases to about 1.7 μm. Singh has demonstrated similar range of surface roughness of polyjet-printed material (0.68 μm) printed at 0° inclined angle (Singh 2011). This shows that polyjet-printed material displays surface roughness in the submicron range.

In comparison, the FDM printer generates much rougher surfaces where the profile is characterized by a stepping feature. On the contrary to the trend shown for polyjet printers, Ra values decrease at increasing wall angle, and range from 42.97 to 3.24 μm, whereas at 90°, there is a sudden jump in the roughness value to 12.6 μm. Referring to Fig. 7c, the increase in Ra at 90° is due to the stacking layers of the printed materials. The Ra values of FDM-printed parts was verified based on the definition of average Ra for each sloping angle θ at the preset layer thickness t of 178 μm. Besides straight channels, surface characteristics at different turning and slanting angles were visually examined (Fig. 9).

Due to the novel nature of the technique, the printed parts' surface structuring and the effect on the performance of microfluidic devices is less studied. Comparing with the Ra of <1 nm produced by photolithography using PDMS, both printers are much inferior with the use of the current model materials. However, the results do not serve to refute the feasibility of 3D printing as a candidate for biological microfluidic devices due to the following reasons.

Firstly, the amount of surface patterning and roughness desired depends on the application. A case in point is the mixers, where complex flows are required to trigger chaotic conditions, as diffusion in laminar flow requires long channels and is highly inefficient. Secondly, Ra values obtained in this study can be improved through post-processing procedures such as surface polishing. Paydar et al. (2014) was able to improve the surface roughness of PMMA-based printed parts by 50 % with the use of wax, though more biologically compatible material is needed for tissue engineering uses. Lastly, the role of surface patterning should not be overrated. Prediction and offset of 3D-printed parts can be employed for functional use (Moore et al. 2011). Though one cannot refute the impact of characteristic surface patterns produced by 3D printers on flow, proper calibration and careful studies may improve performance, depending on the application.

3.5 Water contact angle of printing material

Untreated PDMS is hydrophobic and prone to the nucleation of bubbles within the channel (Anderson et al. 2000b). Wetting at the fluid–wall interface determines the flow pattern. In particular, droplet formation devices produce water-in-oil droplets under hydrophobic surface condition, while oil-in-water droplets are produced in hydrophilic device (Okushima et al. 2004). Surface treatment of the fabricated systems can be performed to enhance surface hydrophobicity. Additionally, surfactants of various concentrations can be added to the fluid phase to enact changes to the solid surface's hydrophobicity (Xu et al. 2006).

From the water contact angle tests, FullCure 720 and ABSplus-P430 are hydrophilic, with average contact angles of 81.0° and 75.5°, respectively. Another polyjet model material, VeroClear, was also tested and was found to be slightly hydrophobic, with an average contact angle of 93.0°.

Water contact angle depends on a number of parameters, including material composition and surface roughness. In this study, only the contact angles on the horizontal planes printed with 0° inclination angle were measured. Also, drop size was known to influence the contact angle due to contact angle hysteresis (Good and Koo 1979; Marmur 1996). For example, another study which measured the contact angle of ABS at a number of drop volumes gave a value of 87.4°, which is 12° higher than that obtained here (Moore et al. 2011). However, a detailed analysis of the contact angles is not the main aim of this study, which is to provide a rough estimate of the surface wetting ability of the model material in comparison with that desired by microfluidic devices. Thus, only drop volume of 5 μl or 2.12 mm in diameter was used.
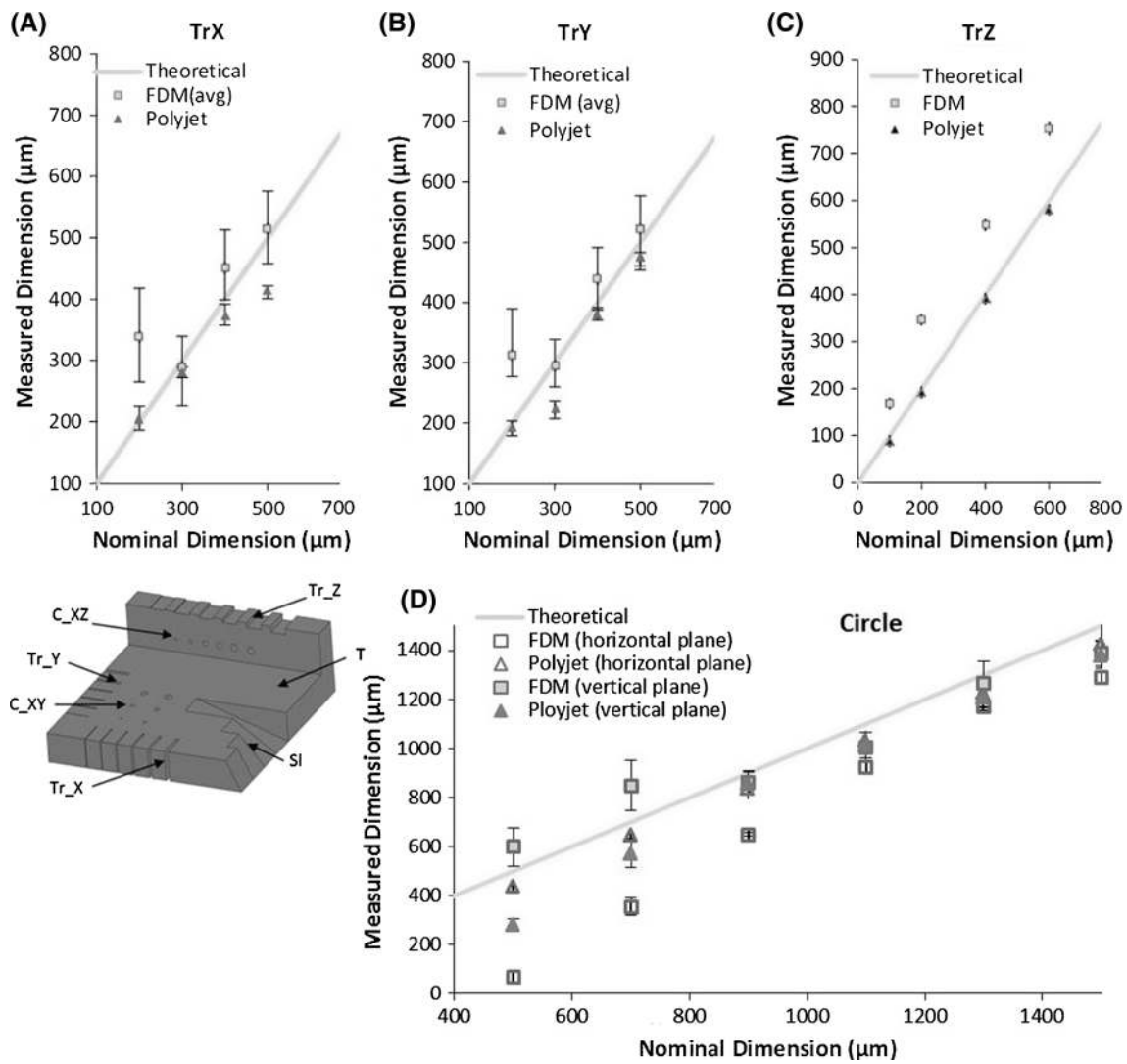
Fig. 5 Measured against nominal dimensions. **a** x-direction, **b** y-direction, **c** z-direction, **d** of circular diameter (theoretical graph slope = 1 for comparison between measured
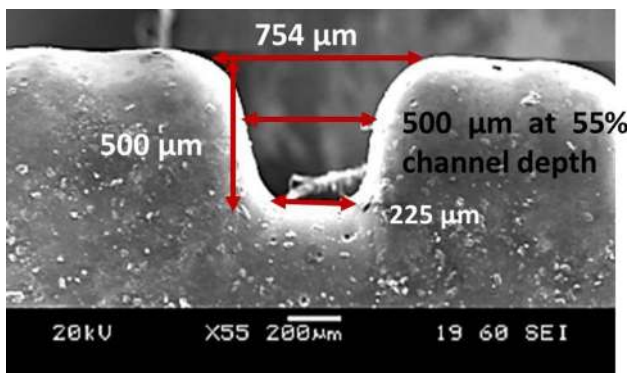

Fig. 6 Distribution of width due to leaning walls

Since hydrophilic surface is preferred in most microfluidic channels, the presently tested model materials are desirable. Though not investigated in this study, larger surface roughness was found to increase hydrophobicity (Chu et al. 2014). Relating to the surface roughness results obtained, increasing the side wall angle may have an undesirable impact on surface properties. For the present case, since the model materials are not highly hydrophilic, rougher surfaces created by increasing wall angles should be avoided. However, just as in the case of surface roughness, wetting ability can be improved by post-processing, and results from these tests only serve as a guide for preliminary design purpose.
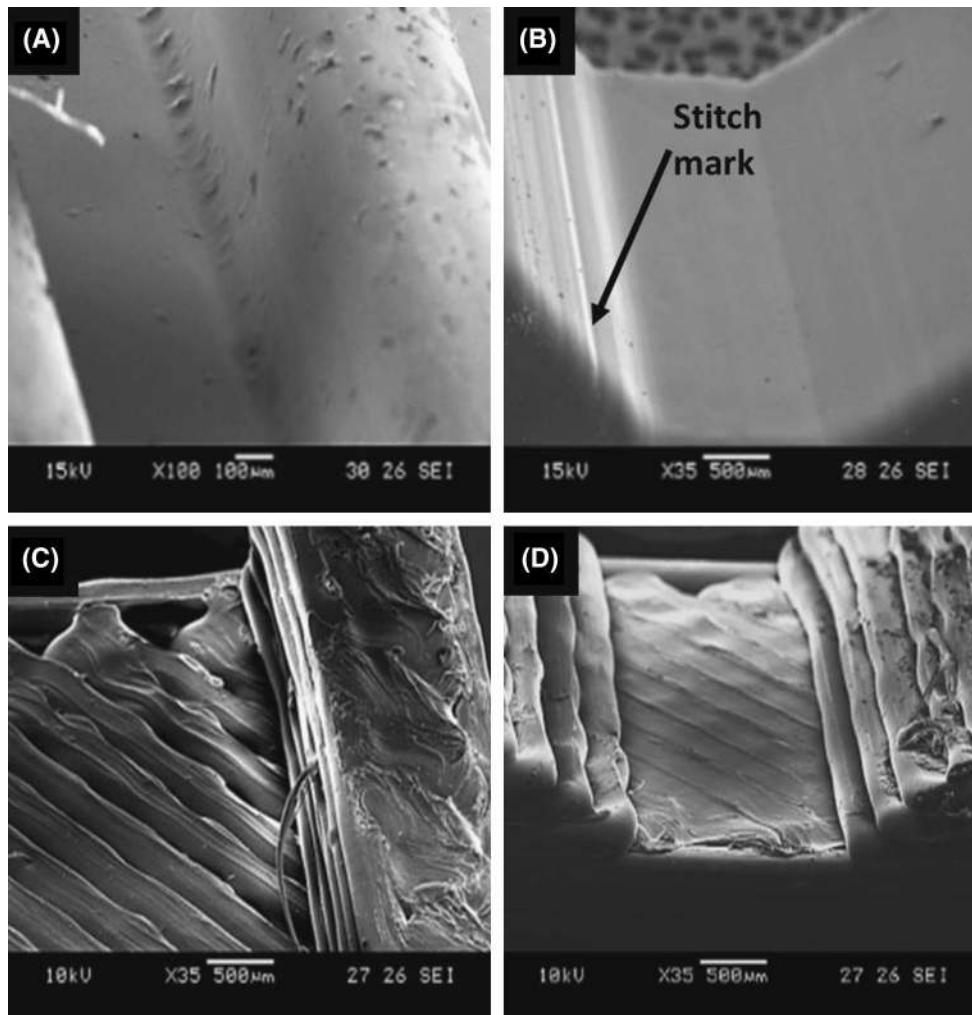
Fig. 7 SEM images of printed channels. **a**, **b** are polyjet-printed channel; **c**, **d** are FDM-printed channel
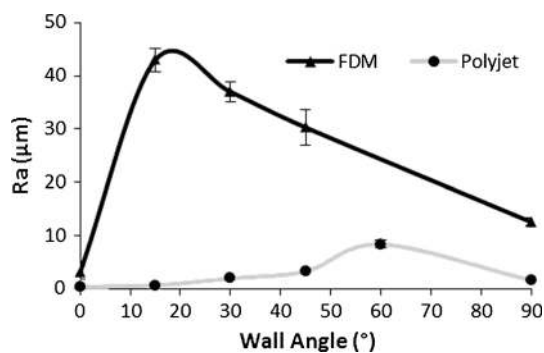

Fig. 8 Ra of the parts printed for various wall angles

3.6 Biocompatibility of model material

The biocompatibility of the build materials is another essential prerequisite for assessing the suitability of microfluidic chip for tissue engineering applications. The biocompatibility of the model material was evaluated quantitatively using a viability assay that is based on cell counting. Both model materials demonstrated good biocompatibility. The control set consisted of cells without any printed part. As shown in Fig. 10, ABSplus-P430 gives consistently high survival rate of above 95 %, comparable with that of the control, across all sterilization conditions, while FullCure 720 exhibited higher mortality rate of about 20 % upon 1 h of UV exposure. Other sterilization method such as high-temperature autoclaving (120 °C, 20 min) is not chosen due to the polymer low melting temperature (~60 °C for Fullcure 720).

The higher cell death after UV treatment could be due to the release of free radicals by FullCure 720, a photopolymer resin. While the constituents of Fullcure 720 are unknown, free radical is a common concern associated with photopolymerizable hydrogel in tissue engineering applications, where photoinitiator concentration is a key parameter that compromises cell viability (Mironi-Harpaz
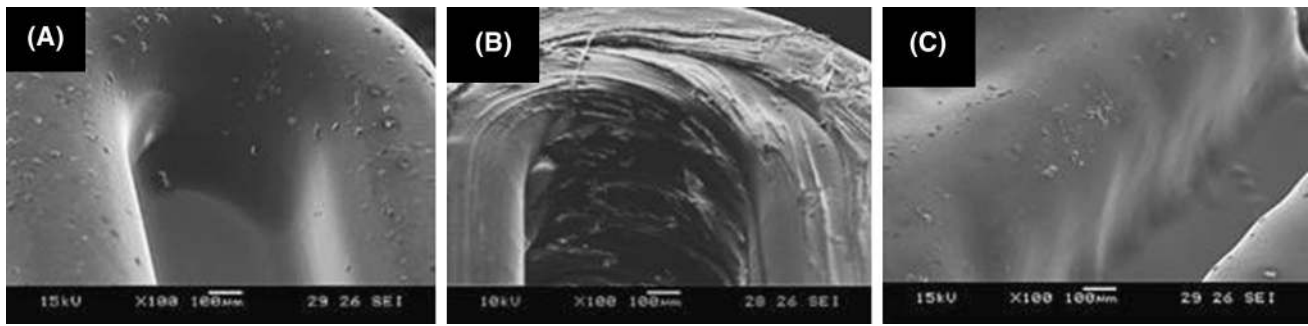
Fig. 9 SEM images of channels. Round channels printed by **a** Polyjet, **b** FDM; **c** Slanting channel by polyjet yielded rougher wall
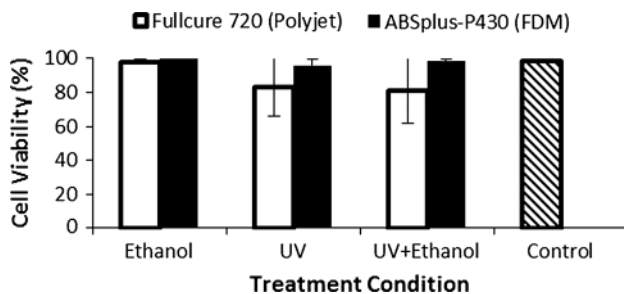

Fig. 10 Cell viability under different treatment conditions

et al. 2012). In this case, exposure to UV irradiation could have caused free radicals, in addition to those already present in the polymer, to be generated, and remnants of these interacted adversely with the cells, leading to detrimental cell death. Despite the difference, cell viabilities for all the treatment conditions are high, indicating the model materials are biocompatible. Future studies may include alternate sterilization techniques such as gamma radiation and electron beams exposure.

4 3D-printed microfluidic devices: case study on rotational flow device and gradient generator

There are three approaches for 3D printing of microfluidic devices, namely (1) direct printing of microchips, (2) direct printing of open-channel microchip, which is bonded to top/bottom layers later, and (3) printing of masters from which microchips can be casted using conventional materials such as PDMS or PMMA. In this study, the first two cases were performed. Of the two printers studied, the polyjet printer was chosen for flow visualization.

To evaluate on the use of three-dimensional printing in microchip fabrication, rotational flow device for generating tissue spheroids (Ota et al. 2010a, b, 2011) and five-layered gradient generator device proposed in (Zhao et al. 2009) were adopted and printed (Figs. 11, 13 respectively).

A minimum channel dimension of 500 μm was used for a small percentage error of about 5 %.

4.1 Direct 3D printing of rotational flow device

A rotational flow device consists of two parallel inlet channels with opposite flows to induce microrotation at high flow rates. Such rotational flow device has been commonly used for rapid formation of tissue spheroids (Hsiao et al. 2009; Ota et al. 2010, 2011; Takai et al. 2013a, b). These rotational flow devices were adapted, drawn, and printed as a unibody via direct 3D printing. There was no bonding or alignment needed in this technique. The design was printed successfully, and the channels designed were clearly visible in the printed physical device. However, we noted several operational concerns. As shown in Fig. 11a, direct printing suffered from difficulty in removing the support materials, as the channels were small and do not allow inflow of solvent for removal of support material. Despite sonication and soaking of the part in the recommended support material solvent sodium hydroxide, the residual of support materials in the channels was observed. Alternatively, a three-layered design was adopted for indirect printing, as shown in Fig. 12.

4.2 3D printing of integrated rotational flow device

The rotational device demonstrated in Fig. 11 was designed with curved serpentine channels. Curved serpentine channels have been used in microfluidic setup to induce cell focusing (Zhang et al. 2014). Figure 12 shows the design with integrated features from both a rotational chamber and serpentine channels. This has demonstrated the greater design freedom in 3D printing where geometrical features can be designed and build within a single setup.

4.3 3D-printed layered gradient generator

The gradient generator proposed by Zhao uses the advantage of three-dimensional designed microfluidic channel

Fig. 11 Direct printing of rotational flow device. **a** Channel blocked by support materials. **b** Channel distorted by material swelling
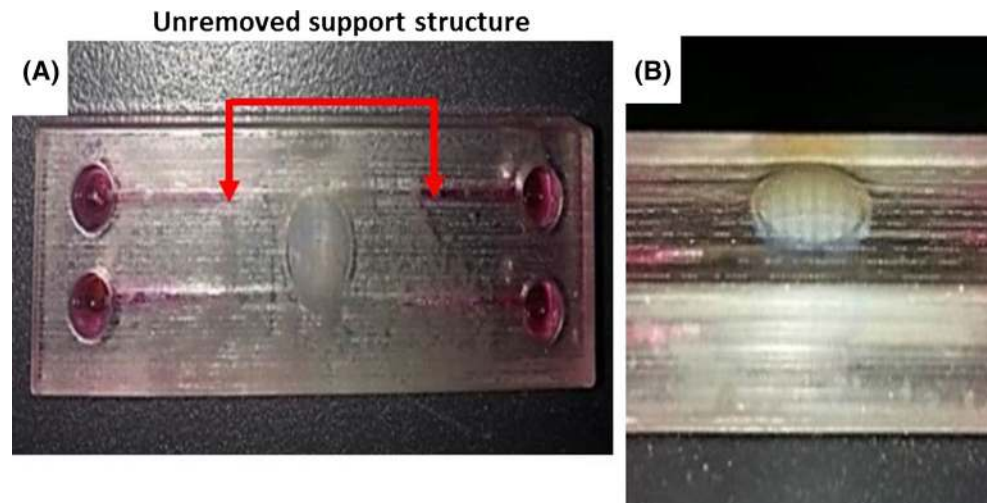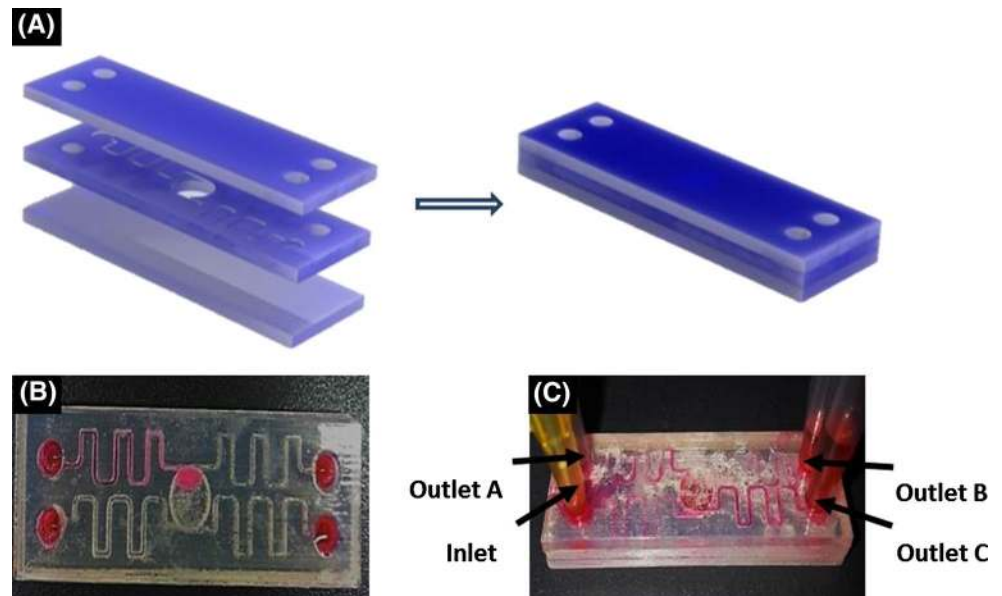

Fig. 12 Printing of layered rotational flow device. **a** Assembly of rotational flow device. **b** Channel blocked by adhesive during bonding. **c** Disturbed flow due to ineffective bonding

for micromixing of chemical (Zhao et al. 2009). The channels were tortuous, at different plane, with connection at turning points for higher chaotic mixing effect. However, the device involved bonding of four different layers to achieve the microchamber mixer. These complex and intricate designs was adapted and printed using 3D printer (Fig. 13). The printed gradient generator demonstrated the ability of fabricating multi-plane complex features within a single build layer.

4.4 Limitations of 3D printing for microfluidic devices

From the feature resolution study, we have designed a minimum channel size of 500 μm for 5 % accuracy to be achieved. The presence of support materials and the lack of effective removal methods are a major engineering and design limitations that compromised the key advantages offered by 3D printing, which are flexibility and structural complexity.

However, one should remain optimistic about the use of 3D printing, as the problems highlighted are not inherent to the technology, but are rather a lack of appropriate materials. Such shortcomings can be eliminated with more specialized machine design (e.g., smaller nozzle size and lateral and vertical displacement of the nozzle heads). Furthermore, there are other printing technologies that are not explored by this study such as stereolithography (SLA) and digital light processing (DLP) (Table 3). In addition, upside-down printing configuration such as DLP facilitates flushing of liquid resin from the solid structure and eases the cleaning process.
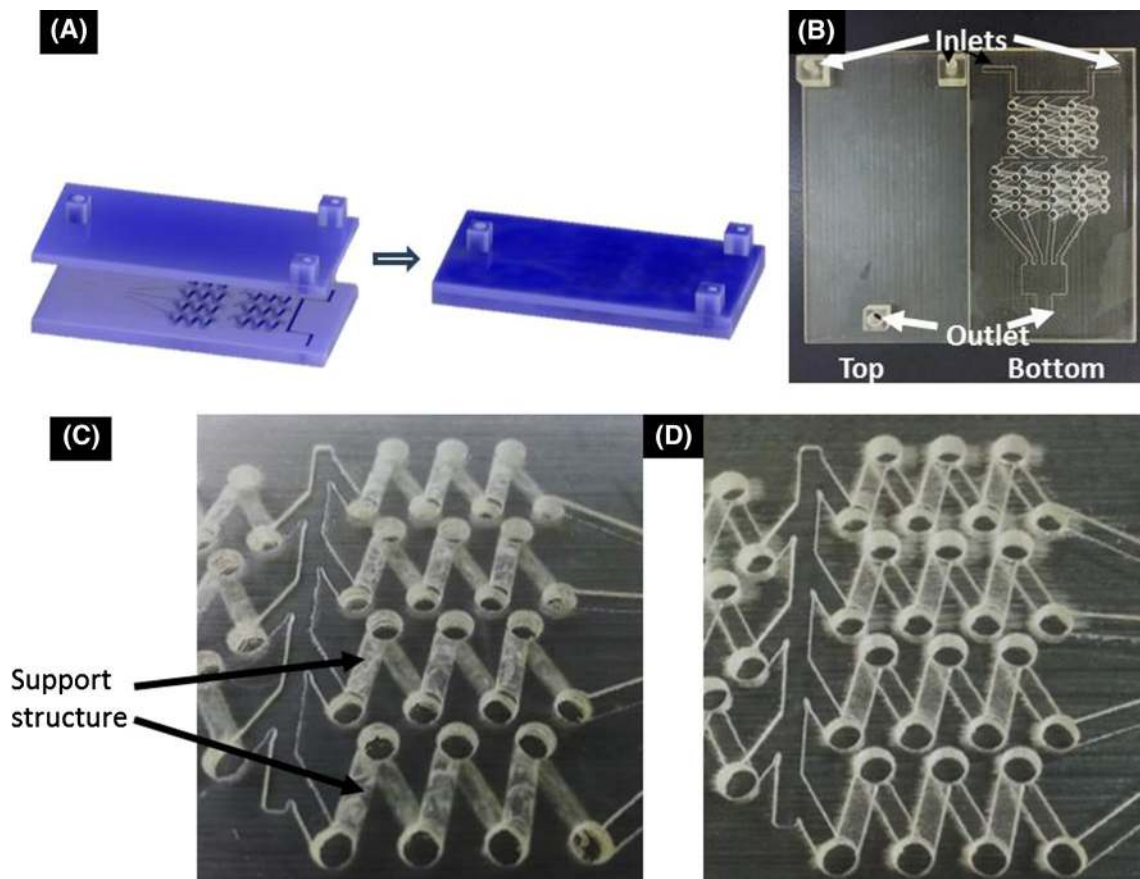
Fig. 13 Assembly of the gradient generator. **a** CAD design of gradient generator. **b** Printed gradient generator. **c** Before and **d** after removal of support material

Table 3 Comparison of the different printing technology

Printer	Resolution	5 % Accuracy	Design limitations	References
FDM	<100 μm unachievable	>1000 μm	Leakage due to filament bonding Opaque material Removal of support structure may be difficult for complex internal features Rough surfaces	Current work and Capel et al. (2013), Polzin et al. (2013), Zhu et al. (2013), Gurrala and Regalla (2014)
Polyjet	<100 μm unachievable	>500 μm	Difficulty in removing support structure for internal features Rough surfaces Material swelling after prolonged soaking in water Limited choice of materials	
SLA	<50 μm in the lateral direction achievable	–	Overcuring of down-facing structures Limited material choice with appropriate viscosity	Capel et al. (2013), Choi et al. (2009), Feng et al. (2015), Shallan et al. (2014)
DLP	<250 μm	–	Limited choice material	Rogers et al. (2015), Shallan et al. (2014)

5 Conclusions

We described the design, fabrication, and characterization of 3D-printed microfluidic chip in this paper to evaluate the applicability of D printing technologies for making tissue engineering-based microfluidic platforms. We fabricated common microfluidic features such as channels, slopes, and circular hole using two most widely used techniques, namely inkjet printing and filament-based deposition. We compared the printing resolution, accuracy, and repeatability of the printed part. Surface roughness and water wetting ability were evaluated. Biocompatibility of the printed pieces under a number of treatment conditions was investigated.

We have shown that resolution of polyjet printing is superior in all axes than FDM. Polyjet-printed parts can be printed with nominal x and z dimensions of 500 and 100 µm with observable features were formed. The polyjet printer produced better spatial accuracy in all three axes with an average deviation of 25.2 µm across all measurement series, as compared to 67.8 µm for FDM. The polyjet printer produces smooth features with surface roughness measurement of 0.47 µm as opposed to FDM-printed parts of 42.97 µm. Model materials from the two systems demonstrated good biocompatibility of above 90 % dependant on the sterilization technique used. We also highlighted the operation consideration of creating 3D-printed microfluidic device such as removal of materials and surface finishing of the device. 3D printing offers the advantage of simplified process chain and the possibility for fabricating complex multilevel systems.

Future works should capitalize further on the idea of 3D printing, developing specialized printers and materials for specific microfluidic applications, and this will ensure that the printed device will be compatible with the intended microfluidic applications in terms of material availability, transparency and strength.

Compliance with ethical standards

Conflict of interest   The authors do not have conflict of interest to declare.

References

Anderson JR, Chiu DT, Jackman RJ, Cherniavskaya O, McDonald JC, Wu H, Whitesides GM (2000a) Fabrication of topologically complex three-dimensional microfluidic systems in PDMS by rapid prototyping. Anal Chem 72(14):3158–3164

Anderson JR, Chiu DT, Wu H, Schueller OJ, Whitesides GM (2000b) Fabrication of microfluidic systems in poly (dimethylsiloxane). Electrophoresis 21:27–40

Au AK, Bhattacharjee N, Horowitz LF, Chang TC, Folch A (2015) 3D-printed microfluidic automation. Lab Chip 15(8):1934–1941. doi:10.1039/C5LC00126A

Benavente-Babace A, Gallego-Perez D, Hansford DJ, Arana S, Perez-Lorenzo E, Mujika M (2014) Single-cell trapping and selective treatment via co-flow within a microfluidic platform. Biosens Bioelectron 61:298–305. doi:10.1016/j.bios.2014.05.036

Bhagat AAS, Kuntaegowdanahalli SS, Papautsky I (2008) Continuous particle separation in spiral microchannels using dean flows and differential migration. Lab Chip 8(11):1906–1914. doi:10.1039/b807107a

Capel AJ, Edmondson S, Christie SD, Goodridge RD, Bibb RJ, Thurstans M (2013) Design and additive manufacture for flow chemistry. Lab Chip 13(23):4583–4590

Chan HF, Zhang Y, Ho Y-P, Chiu Y-L, Jung Y, Leong KW (2013) Rapid formation of multicellular spheroids in double-emulsion droplets with controllable microenvironment. Sci Rep. doi:10.1038/srep03462

Choi J-W, Wicker RB, Cho S-H, Ha C-S, Lee S-H (2009) Cure depth control for complex 3D microstructure fabrication in dynamic mask projection microstereolithography. Rapid Prototyp J 15(1):59–70

Chu D, Nemoto A, Ito H (2014) Effects of geometric parameters for superhydrophobicity of polymer surfaces fabricated by precision tooling machines. Microsyst Technol 20(2):193–200. doi:10.1007/s00542-013-1758-3

Chua C-K, Yeong W-Y, Leong K-F (2005) Rapid prototyping in tissue engineering: a state-of-the-art report. In: Virtual modelling and rapid manufacturing—advanced research in virtual and rapid prototyping, pp 19–27

Cui X, Dean D, Ruggeri ZM, Boland T (2010) Cell damage evaluation of thermal inkjet printed Chinese hamster ovary cells. Biotechnol Bioeng 106(6):963–969

Feng Z, Skommer J, Macdonald NP, Friedrich T, Kaslin J, Wlodkowic D (2015) Three-dimensional printed millifluidic devices for zebrafish embryo tests. Biomicrofluidics 9(4):1–10. doi:10.1063/1.4927379

Fiorini GS, Chiu DT (2005) Disposable microfluidic devices: fabrication, function, and application. Biotechniques 38(3):429–446

Good RJ, Koo M (1979) The effect of drop size on contact angle. J Colloid Interface Sci 71(2):283–292

Gurrala PK, Regalla SP (2014) Part strength evolution with bonding between filaments in fused deposition modelling. Virtual Phys Prototyp 9(3):141–149. doi:10.1080/17452759.2014.913400

Ho C-M, Tai Y-C (1998) Micro-electro-mechanical-systems (MEMS) and fluid flows. Annu Rev Fluid Mech 30(1):579–612

Holmes D, Whyte G, Bailey J, Vergara-Irigaray N, Ekpenyong A, Guck J, Duke T (2014) Separation of blood cells with differing deformability using deterministic lateral displacement. Interface Focus 4(6):20140011

Hsiao AY, Torisawa Y-S, Tung Y-C, Sud S, Taichman RS, Pienta KJ, Takayama S (2009) Microfluidic system for formation of PC-3 prostate cancer co-culture spheroids. Biomaterials 30(16):3020–3027. doi:10.1016/j.biomaterials.2009.02.047

Huang LR, Cox EC, Austin RH, Sturm JC (2004) Continuous particle separation through deterministic lateral displacement. Science 304(5673):987–990. doi:10.1126/science.1094567

Huang Y, Liu S, Yang W, Yu C (2010) Surface roughness analysis and improvement of PMMA-based microfluidic chip chambers by CO_2 laser cutting. Appl Surf Sci 256(6):1675–1678

Ismagilov RF, Rosmarin D, Kenis PJA, Chiu DT, Zhang W, Stone HA, Whitesides GM (2001) Pressure-driven laminar flow in tangential microchannels: an elastomeric microfluidic switch. Anal Chem 73(19):4682–4687. doi:10.1021/ac010374q

Kang E, Jeong GS, Choi YY, Lee KH, Khademhosseini A, Lee S-H (2011) Digitally tunable physicochemical coding of material composition and topography in continuous microfibres. Nat Mater 10(11):877–883

Khoo ZX, Teoh JEM, Liu, Y, Chua CK, Yang S, An J, Leong, KF, Yeong WY (2015) 3D printing of smart materials: a review on recent progresses in 4D printing. Virtual Phys Prototyp 10(3):103–122. doi:10.1080/17452759.2015.1097054

Kuo C-T, Chiang C-L, Chang C-H, Liu H-K, Huang G-S, Huang RY-J, Wo AM (2014) Modeling of cancer metastasis and drug resistance via biomimetic nano-cilia and microfluidics. Biomaterials 35(5):1562–1571. doi:10.1016/j.biomaterials.2013.11.008

Lee JM, Yeong WY (2015) A preliminary model of time-pressure dispensing system for bioprinting based on printing and material parameters. Virtual Phys Prototyp 10(1):3–8. doi:10.1080/17452759.2014.979557

Liao Y, Song J, Li E, Luo Y, Shen Y, Chen D, Midorikawa K (2012) Rapid prototyping of three-dimensional microfluidic mixers in glass by femtosecond laser direct writing. Lab Chip 12(4):746–749

Takai H, Kojima M, Ohara K, Horade M, Tanikawa T, Mae Y, IEEE (2013) Microfluidic device for automated generation of toroidal-like spheroids. In: 2013 10th international conference on ubiquitous robots and ambient intelligence, pp 140–143

Malda J, Visser J, Melchels FP, Jüngst T, Hennink WE, Dhert WJ, Hutmacher DW (2013) 25th anniversary article: engineering hydrogels for biofabrication. Adv Mater 25(36):5011–5028

Marmur A (1996) Equilibrium contact angles: theory and measurement. Colloids Surf A 116(1–2):55–61. doi:10.1016/0927-7757(96)03585-6

McDonald JC, Chabinyc ML, Metallo SJ, Anderson JR, Stroock AD, Whitesides GM (2002) Prototyping of microfluidic devices in poly(dimethylsiloxane) using solid-object printing. Anal Chem 74(7):1537–1545. doi:10.1021/ac010938q

Mironi-Harpaz I, Wang DY, Venkatraman S, Seliktar D (2012) Photopolymerization of cell-encapsulating hydrogels: crosslinking efficiency versus cytotoxicity. Acta Biomater 8(5):1838–1848. doi:10.1016/j.actbio.2011.12.034

Moltzahn F, Olshen AB, Baehner L, Peek A, Fong L, Stöppler H, Blelloch R (2011) Microfluidic-based multiplex qRT-PCR identifies diagnostic and prognostic microRNA signatures in the sera of prostate cancer patients. Cancer Res 71(2):550–560. doi:10.1158/0008-5472.can-10-1229

Moore J, McCuiston A, Mittendorf I, Ottway R, Johnson RD (2011) Behavior of capillary valves in centrifugal microfluidic devices prepared by three-dimensional printing. Microfluid Nanofluid 10(4):877–888. doi:10.1007/s10404-010-0721-1

Nagrath S, Sequist LV, Maheswaran S, Bell DW, Irimia D, Ulkus L, Toner M (2007) Isolation of rare circulating tumour cells in cancer patients by microchip technology. Nature 450(7173):U1235–U1240. doi:10.1038/nature06385

Novik E, Maguire TJ, Chao P, Cheng KC, Yarmush ML (2010) A microfluidic hepatic coculture platform for cell-based drug metabolism studies. Biochem Pharmacol 79(7):1036–1044. doi:10.1016/j.bcp.2009.11.010

Okushima S, Nisisako T, Torii T, Higuchi T (2004) Controlled production of monodisperse double emulsions by two-step droplet breakup in microfluidic devices. Langmuir 20(23):9905–9908. doi:10.1021/la0480336

Onoe H, Okitsu T, Itou A, Kato-Negishi M, Gojo R, Kiriya D, Kuribayashi-Shigetomi K (2013) Metre-long cell-laden microfibres exhibit tissue morphologies and functions. Nat Mater 12(6):584–590

Ota H, Kodama T, Miki N (2010a) Microfluidic experimental array using micro-rotation flow for producing size-controlled three-dimensional spheroids. Paper presented at the 2010 International Symposium on Micro-NanoMechatronics and Human Science (MHS), 7–10 Nov 2010

Ota H, Yamamoto R, Deguchi K, Tanaka Y, Kazoe Y, Sato Y, Miki N (2010b) Three-dimensional spheroid-forming lab-on-a-chip using micro-rotational flow. Sens Actuators B 147(1):359–365. doi:10.1016/j.snb.2009.11.061

Ota H, Kodama T, Miki N (2011) Rapid formation of size-controlled three dimensional hetero-cell aggregates using micro-rotation flow for spheroid study. Biomicrofluidics. doi:10.1063/1.3609969

Paydar OH, Paredes CN, Hwang Y, Paz J, Shah NB, Candler RN (2014) Characterization of 3D-printed microfluidic chip interconnects with integrated O-rings. Sens Actuators A 205:199–203. doi:10.1016/j.sna.2013.11.005

Polzin C, Spath S, Seitz H (2013) Characterization and evaluation of a PMMA-based 3D printing process. Rapid Prototyp J 19(1):37–43

Rival A, Jary D, Delattre C, Fouillet Y, Castellan G, Bellemin-Comte A, Gidrol X (2014) An EWOD-based microfluidic chip for single-cell isolation, mRNA purification and subsequent multiplex qPCR. Lab Chip 14(19):3739–3749. doi:10.1039/C4LC00592A

Rogers CI, Qaderi K, Woolley AT, Nordin GP (2015) 3D printed microfluidic devices with integrated valves. Biomicrofluidics 9(1):016501. doi:10.1063/1.4905840

Sakai S, Ito S, Inagaki H, Hirose K, Matsuyama T, Taya M, Kawakami K (2011) Cell-enclosing gelatin-based microcapsule production for tissue engineering using a microfluidic flow-focusing system. Biomicrofluidics. doi:10.1063/1.3516657

Schrott W, Slouka Z, Červenka P, Ston J, Nebyla M, Přibyl M, Šnita D (2009) Study on surface properties of PDMS microfluidic chips treated with albumin. Biomicrofluidics 3(4):044101

Shallan AI, Smejkal P, Corban M, Guijt RM, Breadmore MC (2014) Cost-effective three-dimensional printing of visibly transparent microchips within minutes. Anal Chem 86(6):3124–3130. doi:10.1021/ac4041857

Shen F, Li X, Li PCH (2014) Study of flow behaviors on single-cell manipulation and shear stress reduction in microfluidic chips using computational fluid dynamics simulations. Biomicrofluidics 8(1):014109. doi:10.1063/1.4866358

Shih SCC, Barbulovic-Nad I, Yang X, Fobel R, Wheeler AR (2013) Digital microfluidics with impedance sensing for integrated cell culture andanalysis. Biosens Bioelectron 42:314–320. doi:10.1016/j.bios.2012.10.035

Sing SL, An J, Yeong WY, Wiria FE (2015) Laser and electron-beam powder-bed additive manufacturing of metallic implants: a review on processes, materials and designs. J Orthop Res. doi:10.1002/jor.23075

Singh R (2011) Process capability study of polyjet printing for plastic components. J Mech Sci Technol 25(4):1011–1015. doi:10.1007/s12206-011-0203-8

Sun J, He Y, Tao W, Yin X, Wang H (2012) Roughness effect on flow and thermal boundaries in microchannel/nanochannel flow using molecular dynamics-continuum hybrid simulation. Int J Numer Methods Eng 89(1):2–19. doi:10.1002/nme.3229

Takai H, Kojima M, Ohara K, Horade M, Tanikawa T, Mae Y, Arai T (2013) Microfluidic device for automated generation of toroidal-like spheroids. Paper presented at the 2013 10th International Conference on Ubiquitous Robots and Ambient Intelligence (URAI), 30 Oct 2013–2 Nov 2013

Vaezi M, Yang S (2015) A novel bioactive PEEK/HA composite with controlled 3D interconnected HA network. Int J Bioprinting 1(1):66–76. doi:10.18063/IJB.2015.01.004

Wang C-C, Yang K-C, Lin K-H, Liu H-C, Lin F-H (2011) A highly organized three-dimensional alginate scaffold for cartilage tissue engineering prepared by microfluidic technology. Biomaterials 32(29):7118–7126

Wang S, Lee JM, Yeong WY (2015) Smart hydrogels for 3D bioprinting. Int J Bioprinting 1:3–14. doi:10.18063/IJB.2015.01.005

Wu LY, Di Carlo D, Lee LP (2008) Microfluidic self-assembly of tumor spheroids for anticancer drug discovery. Biomed Microdevices 10(2):197–202. doi:10.1007/s10544-007-9125-8

Xu JH, Li SW, Tan J, Wang YJ, Luo GS (2006) Controllable preparation of monodisperse O/W and W/O emulsions in the same

microfluidic device. Langmuir 22(19):7943–7946. doi:10.1021/la0605743

Yamada M, Nakashima M, Seki M (2004) Pinched flow fractionation: continuous size separation of particles utilizing a laminar flow profile in a pinched microchannel. Anal Chem 76(18):5465–5471. doi:10.1021/ac049863r

Yan J, Pedrosa VA, Enomoto J, Simonian AL, Revzin A (2011) Electrochemical biosensors for on-chip detection of oxidative stress from immune cells. Biomicrofluidics. doi:10.1063/1.3624739

Yap YL, Yeong WY (2015) Shape recovery effect of 3D printed polymeric honeycomb. Virtual Physic Prototyp 10(2):91–99. doi:10.1080/17452759.2015.1060350

Yeong WY, Chua CK, Leong KF, Chandrasekaran M (2004) Rapid prototyping in tissue engineering: challenges and potential. Trends Biotechnol 22(12):643–652. doi:10.1016/j.tibtech.2004.10.004

Yeong W-Y, Chua C-K, Leong K-F, Chandrasekaran M, Lee M-W (2005) Development of scaffolds for tissue engineering using a 3D inkjet model maker. In: Virtual modelling and rapid manufacturing-advanced research in virtual and rapid prototyping, pp 115–118

Yeong WY, Yap CY, Mapar M, Chua CK (2014) State-of-the-art review on selective laser melting of ceramics. In: High value manufacturing: advanced research in virtual and rapid prototyping, pp 65–70. doi:10.1201/b15961-14

Young EWK, Beebe DJ (2010) Fundamentals of microfluidic cell culture in controlled microenvironments. Chem Soc Rev 39(3):1036–1048. doi:10.1039/B909900J

Yu L, Chen MCW, Cheung KC (2010) Droplet-based microfluidic system for multicellular tumor spheroid formation and anti-cancer drug testing. Lab Chip 10(18):2424–2432. doi:10.1039/c004590j

Zhang J, Yan S, Sluyter R, Li W, Alici G, Nguyen N-T (2014) Inertial particle separation by differential equilibrium positions in a symmetrical serpentine micro-channel. Sci Rep. doi:10.1038/srep04527

Zhao S, Cong H, Pan T (2009) Direct projection on dry-film photoresist (DP 2): do-it-yourself three-dimensional polymer microfluidics. Lab Chip 9(8):1128–1132

Zhu F, Macdonald NP, Cooper JM, Wlodkowic D (2013) Additive manufacturing of lab-on-a-chip devices: promises and challenges. In: Proceedings of SPIE-the international society for optical engineering, art. no. 892344. doi: 10.1117/12.2033400